








RESEARCH ARTICLE | NOVEMBER 30 2023

Micro-DC rotary-motor working smoothly with neither contact brush nor fixed-axis

Shusuke Ishida  ; Satoshi Takatori   ; Ken Hirano  ; Daigo Yamamoto  ; Yohei Oe  ; Kenichi Yoshikawa 

 Check for updates

AIP Advances 13, 115231 (2023)

<https://doi.org/10.1063/5.0169304>



View Online



Export Citation

CrossMark



AIP Advances

Special Topic: Machine Vision, Optical Sensing and Measurement

Submit Today



Micro-DC rotary-motor working smoothly with neither contact brush nor fixed-axis

Cite as: AIP Advances 13, 115231 (2023); doi: 10.1063/5.0169304
Submitted: 30 July 2023 • Accepted: 3 November 2023 •
Published Online: 30 November 2023



Shusuke Ishida,¹ Satoshi Takatori,^{2,3,a)} Ken Hirano,⁴ Daigo Yamamoto,⁵ Yohei Oe,²
and Kenichi Yoshikawa^{2,6}

AFFILIATIONS

¹Division of Material Science, Nara Institute of Science and Technology (NAIST), Nara 630-0192, Japan

²Faculty of Life and Medical Sciences, Doshisha University, Kyoto 610-0394, Japan

³Research Organization of Science and Technology, Ritsumeikan University, Shiga 525-8577, Japan

⁴Health and Medical Research Institute, National Institute of Advanced Industrial Science and Technology (AIST), Takamatsu, Kagawa 761-0395, Japan

⁵Department of Chemical Engineering and Materials Science, Doshisha University, Kyoto 610-0321, Japan

⁶Center for Integrative Medicine and Physics, Institute for Advanced Study, Kyoto University, Kyoto 606-8501, Japan

^{a)} Author to whom correspondence should be addressed: stakator@mail.doshisha.ac.jp

ABSTRACT

Successful construction of a simple sub-millimeter micromotor is reported, which operates under stationary direct current (DC) voltage, with neither a fixed rotational axis nor contacting brush. The screw-shaped chiral rotor undergoes a spinning motion when stationary DC voltage is applied using a pair of cone-shaped electrodes with a staggered arrangement. Analysis of the fluid motion revealed the occurrence of inward-swirling flow in between the electrode tips, which generates a stable spinning motion under the DC voltage. This simple DC micromotor could be beneficial for the advancement of microfluidics, microrobots, etc.

© 2023 Author(s). All article content, except where otherwise noted, is licensed under a Creative Commons Attribution (CC BY) license (<http://creativecommons.org/licenses/by/4.0/>). <https://doi.org/10.1063/5.0169304>

Microfluidics have been actively developed over the past several decades, and further improvements are expected.^{1–4} Although the generation of fluidic motion has been usually managed by connecting with an outer pumping system, it would be beneficial if a micromotor below the size of sub-millimeter would become available. A continuous energy supply is needed to drive micro-objects on the order of tens to hundreds of micrometers because viscosity or dissipation becomes more significant than inertia for motion in a microfluidic system, with a Reynolds number of $Re \ll 1$. This serious frictional/viscous effect is different from the situation in currently available macroscopic electronic motors or other mechanical machines. The significant viscous effect makes downsizing currently available motors or pumps difficult. On the other hand, biological systems use motile micro-machines such as flagella, cilia, and other locomotive apparatus, which work smoothly through the dissipation of chemical energy (e.g., ATP hydrolysis).^{5–8} Generating artificial micromotors under a large viscous effect ($Re \ll 1$) is

scientifically and technologically important, and several attempts have been reported. Regarding the phenomenon of self-rotation driven by direct current (DC) electrical potential in micro-scale, Quincke rotation is well known.^{9–25} Quincke rotation means self-rotation and/or rhythmic motions of solid particles of liquid drops in liquids with weak electrical conductivity driven by a stationary homogeneous DC electric field with a pair of planar/linear electrodes arranged parallel. The underlying mechanism of Quincke rotation has been interpreted in terms of instability of an induced dipole on a particle/droplet surface, which relaxes through mechanical motion. As the extension of the study on Quincke rotation, a directional vectorial motion was observed for micro-particles.⁹ Directional spinning of chiral gear-shaped plastic particles was also reported.²⁶ In contrast to the parallel arrangement of planar or linear electrodes for Quincke rotation, we found that a rhythmic back-and-forth motion for a droplet is generated by adapting a pair of encountering needle shaped electrodes under stationary DC voltage.^{27–29} In

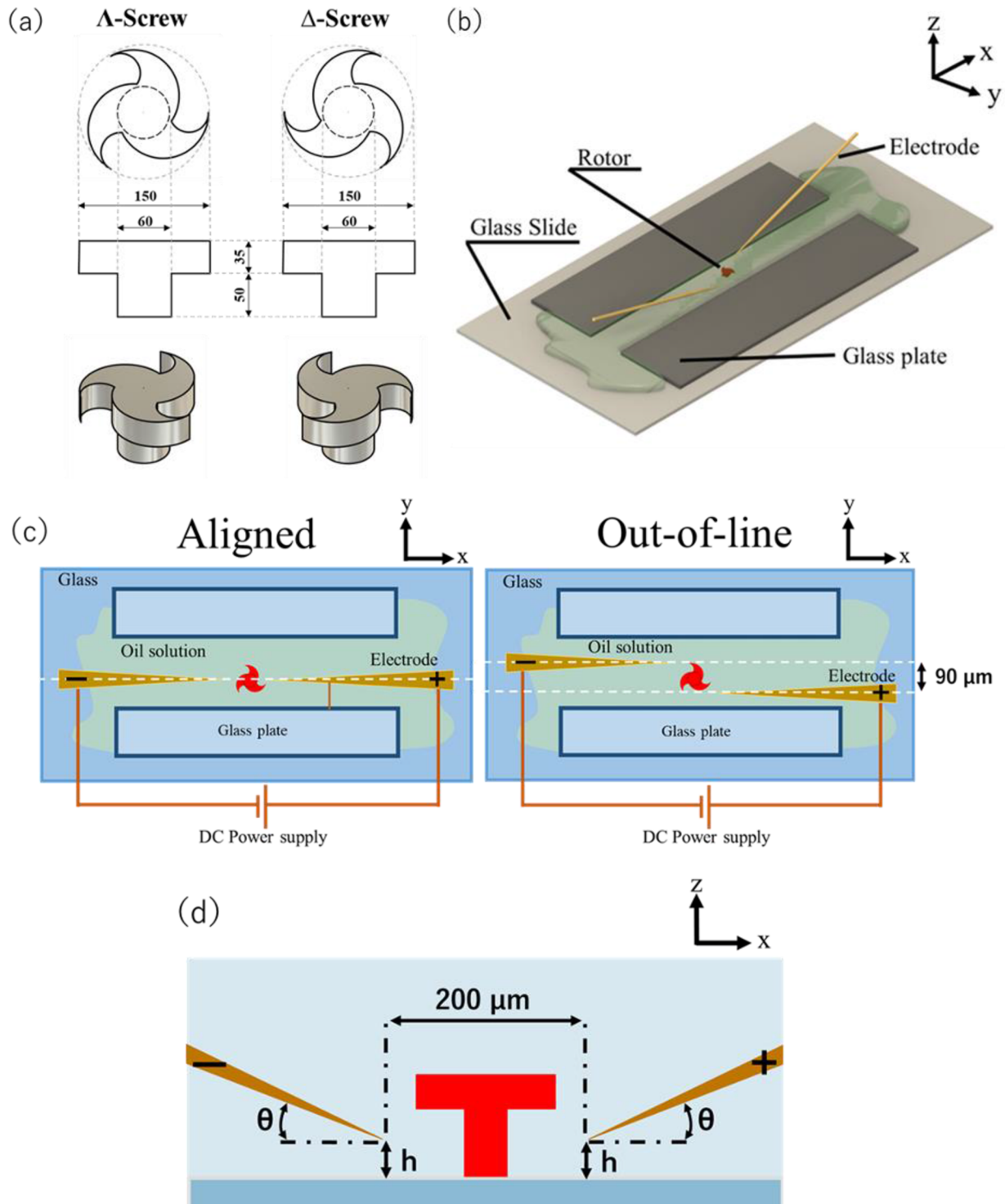


FIG. 1. Schematic representation of the chiral micro-rotor system. (a) Dimensions of the chiral rotors (in μm) used in the present study. Their shapes are nominated as Λ -screw and Δ -screw. The fabrication details are shown in the supplementary material, Figs. S1 and S2. (b) The experimental setup to generate fluidic motions under DC voltage is shown. The micro-rotary motion system operates under a DC electrostatic field in a silicon oil solution containing 17% (v/v) DEPA. The solution height in the region between the pair of the glass plates was ~ 0.2 mm. Smooth and stable rotations were generated on the Δ -screw when electrode pairs were not aligned (out-of-line). (c) Top views of the experimental system where electrodes are in a straight line (aligned) or offset (out-of-line). (d) Side view for either arrangement.

addition, it has been found that orbital and spinning motions of aqueous droplets and solid particles are generated by changing the spatial arrangement of the needle-shaped electrodes.^{30–35} The mechanism on the generation of back-and-forth, orbital and spinning motions has been discussed by considering the effect of dielectric potential in addition to electric potential. As an extension of these studies, here, we report the occurrence of a stable and smooth spinning motion using screw-shaped particles with a chiral symmetry break.

Our experimental design and setup are shown in Fig. 1. Cone-shaped narrow electrodes (Unique Medical, Tokyo, Japan) are shown in yellow. The chiral micro-rotors, Λ -screw and Δ -screw [Fig. 1(a)], were fabricated with an epoxy-based SU-8 photoresist (Micro-Chem, Westborough, MA, USA) using the photolithography method (fabrication procedure is shown in Fig. S1). First, a sacrificial layer was coated onto a silicon wafer of 10 cm diameter with Barrier-Coat No. 6 solution (Shin-Etsu Chemical, Tokyo, Japan). On the silicon wafer, the photoresist SU-8 3010 was coated as the first layer with a thickness of 35 μm . A turbine blade design was patterned on this layer using a UV mask aligner, MA-60F (Mikasa, Tokyo, Japan). A second layer of SU-8 3050 was then coated at a thickness of 50 μm . The shaft portions were patterned onto the second layer with the UV mask aligner. Rotors were developed and removed from the sacrificial layer using an SU-8 developer (Micro-Chem). The developed rotors were washed with isopropanol and ethanol. Approximately 5.1×10^4 particles were obtained from a single silicon wafer (Fig. S2).

The oil phase of the solution was prepared by mixing 100 μl of silicone oil (KF-56, Shin-Etsu Chemical) with 20 μl of di (2-ethylhexyl) phosphate (DEHPA) (97%, Sigma-Aldrich). The ^1H nuclear magnetic resonance (NMR) spectrum of the oil dispersion with DEHPA, thus prepared, is shown in Fig. S3, indicating that the molar ratio between DEHPA and water was 1:15. The chiral micro-rotors were dispersed in the oil phase, followed by mechanical agitation with a vortex mixer for ~ 30 s. Oil solution containing the micro-rotors (20 μl drop) was dripped onto a glass slide. Then the micro-rotor was positioned between the electrodes in the manner schematically represented in Figs. 1(b)–1(d). DC voltage was applied using needle-shaped tungsten electrodes (Unique Medical). These electrodes were placed at the same horizontal level with either an aligned or out-of-line arrangement (discussed further below). The distance between their tips was ~ 200 μm , their height above the glass plate surface, d , was 15 μm , and the insertion angle with respect to the glass plate, θ , was 25° . The motions of the chiral micro-rotors were observed using an optical microscope (IX71, Olympus).

Figure 2(a) exemplifies the spinning motion of the Λ -screw and Δ -screw chiral rotors. Both underwent a clockwise spinning motion under the application of a stationary DC voltage of 100 V. Figure 2(b) shows the spatiotemporal plot for the spinning motion shown in Fig. 2(a). The upper plot indicates that the Λ -screw micro-rotor stably spins by keeping its rotational axis in a fixed position. In contrast, the position of the rotational axis for Δ -screw rotor fluctuated, suggesting that the spinning motion was unstable. Careful inspection of the spatiotemporal diagram of the Δ -screw rotor indicates that the rotor tended to tilt, accompanied by a positional fluctuation of its spinning center, as suggested by the

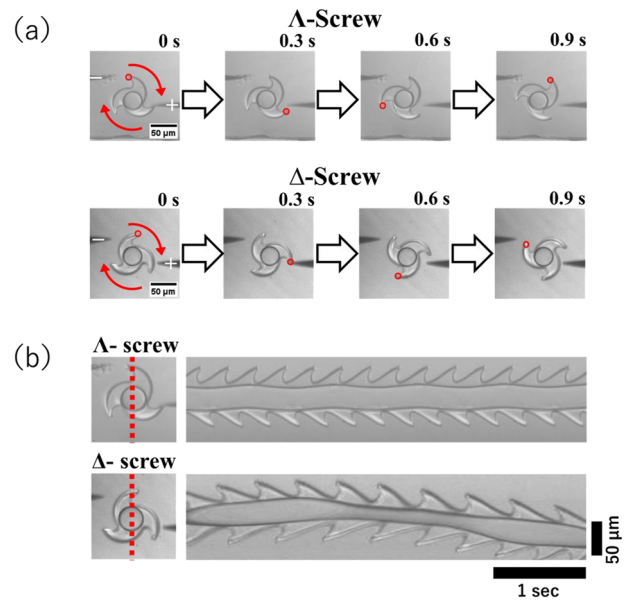


FIG. 2. Rotational motions of the chiral rotors under a DC of 100 V. (a) Time-lapse images of the chiral rotors, Λ -screw (top panel) and Δ -screw (bottom panel). (b) Spatiotemporal diagram of the rotational motions. The Λ -screw exhibited a smooth rotary motion in contrast to the more erratic motion of the Δ -screw.

time-dependent fluctuation of the width of the standing cylinder in the upper view.

Figure 3 shows the voltage dependence of the spinning motion of the chiral micro-rotors, where the measurements were performed with a stepwise 10 V increase, or decrease, in the applied voltage. The Λ -screw micro-rotor began spinning at 90 V, and the spinning frequency increased almost linearly as the voltage increased. No hysteresis was observed when the voltage was decreased from 200 until 90 V. The spinning continued below 90 V and terminated at 60 V, indicating the occurrence of hysteresis in such a voltage region. Contrary to this, the Δ -screw micro-rotor required a greater threshold to begin spinning than the Λ -screw (i.e., 150 vs 90 V for the Λ -screw). When the voltage was decreased, the Δ -screw micro-rotor stopped spinning below 100 V, a larger voltage than that for the Λ -screw (60 V).

We measured the fluid velocity and vorticity to clarify the reason why a stable spinning motion was generated with the Λ -screw and not the Δ -screw. Observations of the fluid motion in the absence of micro-rotors were performed with two types of electrode alignments, “aligned” and “out-of-line.” The particle image velocimetry (PIV) analysis is shown in Fig. 4 [(a) velocity field, \vec{u} , and (b) vorticity lines, $\omega = \text{rot } \vec{u}$]. To obtain these profiles, the open-source code PIVlab³⁶ developed by MATLAB was employed. Liquid flow was generated from the negative electrode side toward the positive electrode side when the electrodes were “aligned” [Fig. 4(a), left]. On the contrary, a single clockwise vortex was formed when the electrodes were arranged as “out-of-line,” where compensation flow appeared in from the side of the positive electrode toward the side of the negative one [Fig. 4(a), right]. The difference between the flow

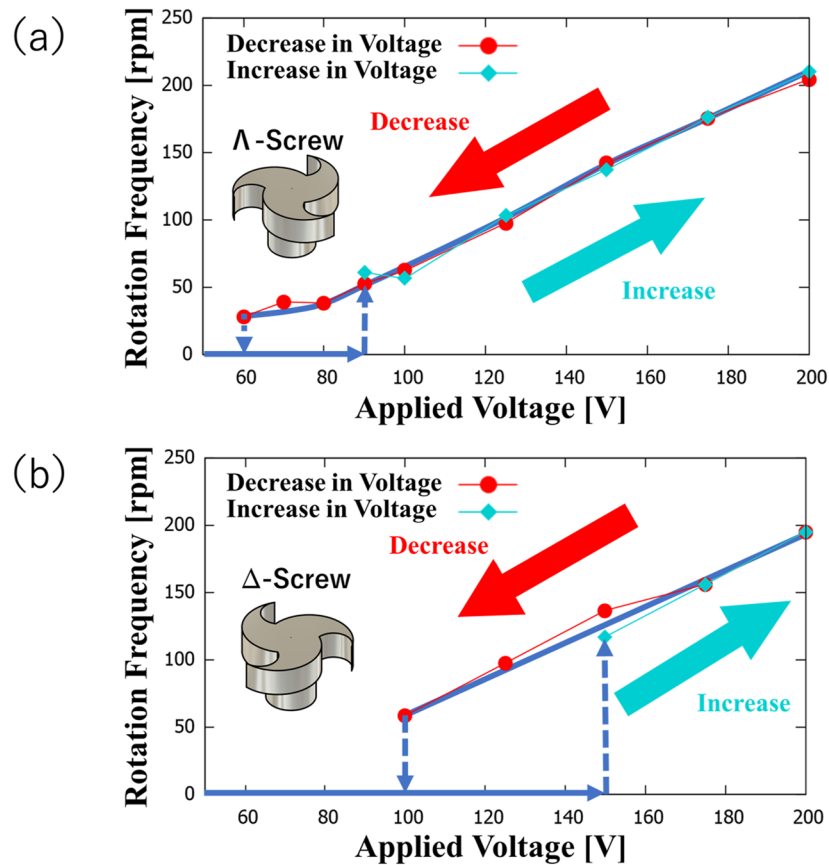


FIG. 3. Mode bifurcation between the stationary and rotating states depending on the magnitude of applied voltage. Rotations were measured under increasing and decreasing applied voltage and indicated the occurrence of hysteresis. Comparison between Λ -screw (a) and Δ -screw (b) indicates that Λ -screw exhibits rotational motion under lower voltage than Δ -screw.

profiles for the electrode arrangements is highlighted in a vortex representation [Fig. 4(b)]. In our previous studies,^{31–33,37} it has been confirmed that silicon oil containing DEPHA causes flow from the negative electrode to the positive one, through the effect of electrophoresis of DEPHA as an anionic surfactant. In other words, assemblies of DEHPA, or reverse micelles, are negatively charged through contact with the negative electrode, and they move toward the positive electrode, which causes the fluid flow shown in Fig. 4. Under the experimental conditions of the present study, the oil phase contained reverse micelles when the molar ratio between DEHPA and water was 1:15, as indicated in Fig. S3. The negative charge of the surfactant molecules is considered to disappear after coming in contact with the positive electrodes, and the resulting non-charging portion in the fluid is driven passively under almost an incompressible condition. The apparent vortex flow, “out-of-line” [right of Fig. 4(a)], was created due to the disparity of the electrode arrangement. It is noted that the generated swirling flow is characterized as a sink, $\text{div } \vec{u} < 0$, with a clockwise rotation. The apparent breakdown of the incompressible condition for the

sink-type vortex suggests the contribution of out of the plane flow; in other words, mild upward flow is generated from the center of the vortex. Based on the above-mentioned considerations, it becomes evident that the stable spinning motion of the Λ -screw is attributed to such a characteristic of the inward vortex flow.

In the present study, the stable spinning motion of a micro-rotor was successfully performed using only a couple of needle-shaped electrodes under a staggered out-of-line arrangement. Neither a spatially fixed axis nor any contact/brush with the electrodes was required. It is expected that the DC voltage would be markedly decreased through the downsizing of the experimental system under a similar electrode arrangement. In relation to this issue, from the study on the generation of rhythmic back-and forth motion under DC voltage,²⁸ it has been demonstrated that the threshold voltage was decreased one order of magnitude from ~ 100 to ~ 10 V when the distance between the electrode tips was decreased from 500 to 10 μm . Further trials to improve the experimental system by downsizing will increase the merit of micro-DC motors and contribute to the advancement of microfluidics.

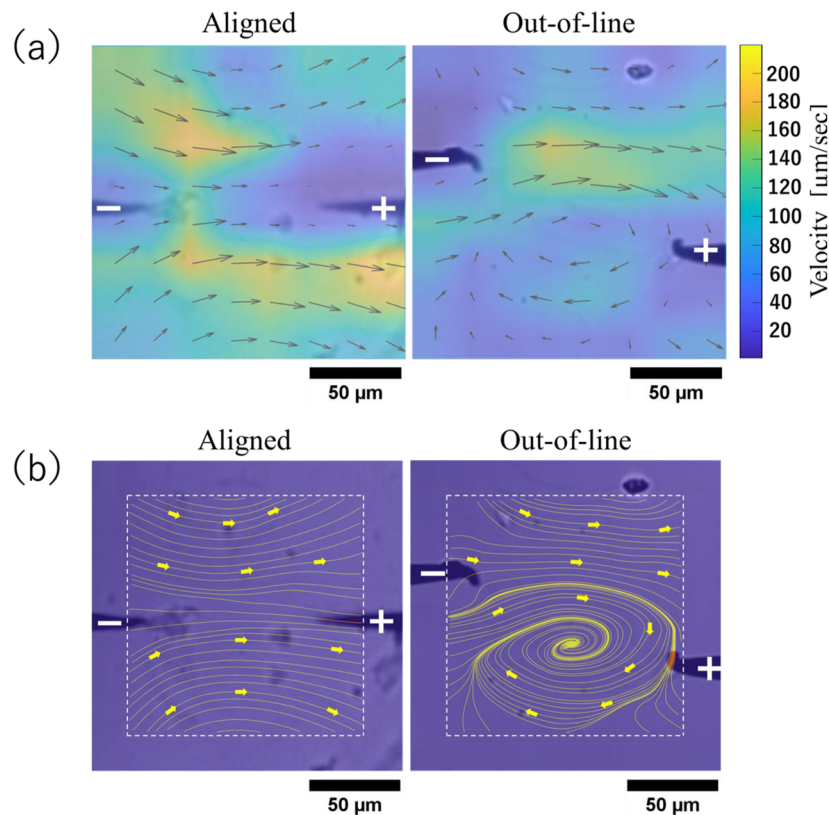


FIG. 4. Particle image velocimetry (PIV) images for electrode arrangements: aligned (left) and out-of-line (right). (a) Velocity and (b) vorticity maps. The region of interest was divided into squares of 150 pixels on the PIV map. The velocity field was calculated at the center of each square using the Fourier transform correlation. The numerical analysis was performed using the PIVlab code, a piece of internal software of MATLAB.³² To visualize the flow profile on the video image, we have added small fragments (below the size of 10 μm) of the mashed rotor into the solution.

See the supplementary material for additional information concerning the detailed procedure of fabrication of rotors (Figs. S1–S2). Figure S3 shows the ^1H NMR spectrum of the solution used in the present study. Movies on the spinning rotors shown in Fig. 2 are given as an mp4 file. VideoS4: Λ -screw spinning at 100 V (mp4). VideoS5: Δ -screw spinning at 100 V (mp4). VideoS6: Λ -screw spinning at 200 V (mp4). VideoS7: Δ -screw spinning at 200 V (mp4).

This work was partially supported by JSPS KAKENHI (Grant No. JP20H01877—K.Y. and Grant No. JP22K06095—K.H.).

AUTHOR DECLARATIONS

Conflict of Interest

The authors have no conflicts to disclose.

Author Contributions

Shusuke Ishida: Conceptualization (equal); Writing – original draft (equal). **Satoshi Takatori:** Conceptualization (equal);

Supervision (equal); Validation (equal); Writing – original draft (equal); Writing – review & editing (equal). **Ken Hirano:** Data curation (equal); Methodology (equal); Resources (equal); Writing – original draft (equal). **Daigo Yamamoto:** Data curation (equal); Methodology (equal); Resources (equal); Validation (equal). **Yohei Oe:** Data curation (equal); Methodology (equal); Resources (equal); Validation (equal). **Kenichi Yoshikawa:** Conceptualization (equal); Data curation (equal); Funding acquisition (equal); Methodology (equal); Resources (equal); Supervision (equal); Validation (equal); Writing – original draft (equal); Writing – review & editing (equal).

DATA AVAILABILITY

The data that support the findings of this study are available from the corresponding author upon reasonable request.

REFERENCES

- ¹D. Baigl, *Lab Chip* **12**, 3637–3653 (2012).
- ²K. Song, G. Li, X. Zu, Z. Du, L. Liu, and Z. Hu, *Micromachines* **11**, 297 (2020).
- ³A. Gergely, B. Sándor, C. Paizs, R. Tötös, and Z. Néda, *Sci. Rep.* **10**, 21305 (2020).
- ⁴T. Nitta, Y. Wang, Z. Du, K. Morishima, and Y. Hiratsuka, *Nat. Mater.* **20**, 1149–1155 (2021).

- ⁵S. Erbas-Cakmak, S. D. Fielden, U. Karaca, D. A. Leigh, C. T. McTernan, D. J. Tetlow, and M. R. Wilson, *Science* **358**, 340–343 (2017).
- ⁶T. Nishizaka, T. Masaike, and D. Nakane, *Biophys. Rev.* **11**, 653–657 (2019).
- ⁷A. Otomo, T. Iida, Y. Okuni, H. Ueno, T. Murata, and R. Iino, *Proc. Natl. Acad. Sci. U. S. A.* **119**, e2210204119 (2022).
- ⁸Y. Hasimoto, M. Sugawa, Y. Nishiguchi, F. Aeba, A. Tagawa, K. Suga, N. Tanaka, H. Ueno, H. Yamashita, R. Yokota *et al.*, *Biophys. J.* **122**, 554–564 (2023).
- ⁹G. Quincke, *Ann. Phys.* **295**, 417–486 (1896).
- ¹⁰J. R. Melcher and G. I. Taylor, *Annu. Rev. Fluid Mech.* **1**, 111–146 (1969).
- ¹¹D. A. Saville, *Annu. Rev. Fluid Mech.* **29**, 27–64 (1997).
- ¹²A. Jáklí, B. Senyuk, G. Liao, and O. D. Lavrentovich, *Soft Matter* **4**, 2471–2474 (2008).
- ¹³A. Bricard, J.-B. Caussin, N. Desreumaux, O. Dauchot, and D. Bartolo, *Nature* **503**, 95–98 (2013).
- ¹⁴A. Bricard, J.-B. Caussin, D. Das, C. Savoie, V. Chikkadi, K. Shitara, O. Chepizhko, F. Peruani, D. Saintillan, and D. Bartolo, *Nat. Commun.* **6**, 7470 (2015).
- ¹⁵M. Ouriemi and P. M. Vlahovska, *Langmuir* **31**, 6298–6305 (2015).
- ¹⁶A. M. Drews, C. A. Cartier, and K. J. Bishop, *Langmuir* **31**, 3808–3814 (2015).
- ¹⁷D. C. Prieve, B. A. Yezer, A. S. Khair, P. J. Sides, and J. W. Schneider, *Adv. Colloid Interface Sci.* **244**, 21–35 (2017).
- ¹⁸Q. Brosseau, G. Hickey, and P. M. Vlahovska, *Phys. Rev. Fluids* **2**, 014101 (2017).
- ¹⁹R. Flittner and M. Přibyl, *J. Fluid Mech.* **822**, 31–53 (2017).
- ²⁰G. E. Pradillo, H. Karani, and P. M. Vlahovska, *Soft Matter* **15**, 6564–6570 (2019).
- ²¹B. Zhang, A. Sokolov, and A. Snezhko, *Nat. Commun.* **11**, 4401 (2020).
- ²²Z. Zhang, H. Yuan, Y. Dou, M. O. de la Cruz, and K. J. M. Bishop, *Phys. Rev. Lett.* **126**, 258001 (2021).
- ²³Z. T. Liu, Y. Shi, Y. Zhao, H. Chaté, X.-q. Shi, and T. H. Zhang, *Proc. Natl. Acad. Sci. U. S. A.* **118**, e2104724118 (2021).
- ²⁴B. Zhang, A. Snezhko, and A. Sokolov, *Phys. Rev. Lett.* **128**, 018004 (2022).
- ²⁵G. Kokot, H. A. Faizi, G. E. Pradillo, A. Snezhko, and P. M. Vlahovska, *Commun. Phys.* **5**, 91 (2022).
- ²⁶M. Zrinyi and M. Nakano, *Period. Polytech., Chem. Eng.* **61**, 15–18 (2017).
- ²⁷M. Hase, S. N. Watanabe, and K. Yoshikawa, *Phys. Rev. E* **74**, 046301 (2006).
- ²⁸T. Kurimura, M. Ichikawa, M. Takinoue, and K. Yoshikawa, *Phys. Rev. E* **88**, 042918 (2013).
- ²⁹Q. Tang, Z. Zhang, J.-H. Zhang, F. Tang, C. Wang, and X. Cui, *Micromachines* **13**, 2229 (2022).
- ³⁰M. Takinoue, Y. Atsumi, and K. Yoshikawa, *Appl. Phys. Lett.* **96**, 104105 (2010).
- ³¹D. Yamamoto, R. Yamamoto, T. Kozaki, A. Shioi, S. Fujii, and K. Yoshikawa, *Chem. Lett.* **46**, 1470–1472 (2017).
- ³²D. Yamamoto, K. Kosugi, K. Hiramatsu, W. Zhang, A. Shioi, K. Kamata, T. Iyoda, and K. Yoshikawa, *J. Chem. Phys.* **150**, 014901 (2019).
- ³³W. Zhang, T. Kozaki, I. Kakimoto, D. Yamamoto, K. Yoshikawa, and A. Shioi, *Colloids Surf., A* **607**, 125496 (2020).
- ³⁴J. Sun, L. Zhang, Y. Zhou, Z. Li, A. Libanori, Q. Tang, Y. Huang, C. Hu, H. Guo, Y. Peng, and J. Chen, *Mater. Today* **58**, 41–47 (2022).
- ³⁵W. Zhang, K. Ohara, Y. Okamoto, E. Nawa-Okita, D. Yamamoto, and A. Shioi, *Colloids Surf., A* **627**, 127197 (2021).
- ³⁶W. Thielicke and E. Stamhuis, *J. Open Res. Software* **2**, e30 (2014).
- ³⁷T. Kurimura, S. Mori, M. Miki, and K. Yoshikawa, *J. Chem. Phys.* **145**, 034902 (2016).